Am J Transl Res 2019;11(1):430-441
www.ajtr.org /ISSN:1943-8141/AJTR0088407

Original Article

Dynamic patterns of H3K4me3, H3K27me3, and Nanog during rabbit embryo development

Jiao Liu[1*], Liyou An[1*], Jiqiang Wang[1], Zhihui Liu[1], Yujian Dai[1], Yanhong Liu[1], Lan Yang[2], Fuliang Du[1,2]

[1]Jiangsu Key Laboratory for Molecular and Medical Biotechnology, College of Life Sciences, Nanjing Normal University, Nanjing 210046, PR China; [2]Lannuo Biotechnologies Wuxi Inc., Wuxi 214000, PR China. [*]Equal contributors.

Received November 14, 2018; Accepted December 14, 2018; Epub January 15, 2019; Published January 30, 2019

Abstract: Epigenetic modification and expression of key pluripotent factors are critical for development, cell fate determination, and differentiation in early embryos. In this study, we systematically examined the dynamic patterns of histone modifications (H3K4me3 and H3K27me3) and Nanog expression during the development of preimplantation rabbit embryos. Rabbit oocytes, 1-, 2-, 4-, 8-, and 16-cell embryos, morulae, and blastocysts were collected at specific time points following superovulation and assessed for nuclear H3K4me3, H3K27me3, and Nanog expression by immunofluorescence microscopy. The frequency of H3K4me3-positive nuclear staining was highest in oocytes through 4-cell embryos (100%), decreased in 8-cell (97.2%) and 16-cell (94.4%) embryos ($P > 0.05$), declined dramatically in morulae (86.7%) (1- through 8-cell embryos vs morulae, $P < 0.05$), and was the lowest in blastocysts (76.2%) ($P < 0.05$). Nuclear staining of H3K27me3 was negative in oocytes and embryos through the 16-cell stage but was positive in 25.9% of morulae and 34.2% of blastocyst ($P < 0.05$). Similarly, rabbit oocytes and embryos through the 16-cell stage did not express Nanog, but Nanog was expressed in 24.9% of morulae and 36.5% of blastocysts ($P < 0.05$). The observed decrease in H3K4me3 and increase in H3K27me3 as development progressed in preimplantation rabbit embryos, together with late Nanog expression, indicates a correlation of these factors with early embryonic cell fate determination and differentiation. Our study provides a specific and dynamic profile of histone modifications and gene expression that will be important for the derivation of rabbit embryonic stem cells and improving rabbit cloning by somatic cell nuclear transfer.

Keywords: Rabbit, embryo development, Nanog, H3K4me3, H3K27me3

Introduction

Early embryo development following fertilization is characterized by dramatic epigenetic changes, including the erasure of DNA methylation from parental genetic material and massive changes in chromatin structure [1, 2]. With the development and application of immunoprecipitation and micro-DNA sequencing, various epigenetic modifications in mammalian embryo development, including those in humans, have been elucidated [3-5]. Using microchip technology and chromatin immunoprecipitation DNA sequencing (ChIP-Seq), the dynamic changes of mouse chromatin histone modifications H3K4me3 and H3K27me3 that occur during early embryo development have been systematically mapped at the genome-wide level [3-5]. Separately, others have analyzed the H3K9me3 histone modification dynamics in mouse embryos and found that the reconstitution of H3K9me3 within long terminal repeats is critical for the activation of transposable elements and heterochromatin regions during the resting stage of early embryonic development [6]. Maps of DNA methylation [7, 8] and histone modification [9] in human early embryos have also been constructed. With the development of genome-wide high-throughput sequencing and combinatorial approaches for studying epigenetic modifications, various epigenetic modifications, such as H3K27me3, H3K4me3, H3K9me3, H3K27ac, and H3K9ac, have been reported to play important roles in the differentiation of embryonic stem cells (ESC) [10-13].

The rabbit is an important model for human diseases [14-17]. We previously reported the

dynamic expression patterns of Oct4, Cdx-2, and acetylated H4K5 during early embryonic development in rabbits. We found that Oct4 expression significantly decreased at the 8-cell stage and progressively increased from the 16-cell to morula to blastocyst stage [18]. These results indicated that rabbit zygotic genome activation (ZGA) initiates at the 8-cell stage, which is similar in timing to ZGA in human embryos [9]. However, the dynamics of other epigenetic modifications, such as H3K4me3 and H3K27me3, have not been clearly elucidated in rabbits. Lepikhov et al. studied the DNA methylation of rabbit embryos and found that the H3K4me3 and H3K27me3 modifications were similar to those in mice and cattle [19]; however, their spatial and temporal patterns remain unclear. We previously reported dynamic and synergistic expression patterns of H4K5ac, the pluripotency gene *Oct4*, and the differentiation gene *Cdx2* in rabbit embryos [20]. Nanog is an embryonic, stem cell-specific transcription factor and is primarily expressed in the early stages of embryonic development and in embryonic germ cells and embryonal tumor cells [21, 22]. However, the detailed dynamics of Nanog expression in rabbit early embryos remain unknown.

In this study, rabbit oocytes, 1-, 2-, 4-, 8-, and 16-cell embryos, morulae, and blastocysts were examined by immunofluorescence microscopy to determine the patterns of two histone modifications, H3K4me3 and H3K27me3, and expression pattern of Nanog during preimplantation embryonic development. Furthermore, in combination with previously published Oct4 expression data [18], correlations between the dynamic histone methylation patterns and expression of the pluripotent factors Oct4 and Nanog in rabbit embryos were elucidated.

Materials and methods

Reagents, animals, and superovulation

Chemicals, unless otherwise noted, were purchased from Sigma-Aldrich (Sigma, St. Louis, MO, USA). All animal experiments were carried out in accordance with the animal experiment operating specifications, and the implementation plan was approved by the Animal Ethics Committee of Nanjing Normal University. New Zealand white rabbits of at least 6 months of age were housed in regular animal facilities with unregulated access to food and water. Female donor rabbits were superovulated using a routine regime [23], consisting of two 3-mg, two 4-mg, and two 5-mg administrations of follicle-stimulating hormone (Folltropin, Bioniche Animal Health Canada, Belleville, Ontario, Canada) at intervals of 12 h, followed by 150 IU of human choriogonadotropin (hCG) (Chorulon, Intervet Inc, Millsboro, DE, USA).

Oocyte and embryo collection

Oocytes were collected from the oviducts of superovulated donors that were not mated with males, 14 h post-hCG injection. Embryos at different stages were collected from superovulated does that had been mated with fertile males by flushing the oviducts with Dulbecco's Phosphate-Buffered Saline (DPBS, 15240-013, Gibco, NY, USA) on specific days following mating, as follows: 1- and 2-cell embryos (Day 1); 4- and 8-cell embryos (Day 2); and 16-cell embryos (Day 3). Morulae (Day 3.5) and blastocysts (Day 4) were flushed from the uterus of the mated donors. Oocytes and embryos were searched and collected under a stereo-microscope, the cumulus cells surrounding oocytes were removed by a glass pipette. Prior to fixation and staining, oocytes and embryos were cultured in 2.5% fetal bovine serum (FBS, SH0070.03, Hyclone, Logan, Utah, USA) B2 medium (Laboratories CCD, Paris, France) under 5% CO_2 incubator with humid air.

Embryo fixation and immunofluorescence staining

The oocytes and embryos were washed 3 to 5 times in DPBS medium containing 0.1% polyvinyl alcohol (PVA, P8136) and were then fixed with 4% paraformaldehyde (16005) in DPBS for 10 min. After subsequent washing in DPBS for 10 min, the fixed oocytes and embryos were permeabilized by incubation in 0.5% Triton-X100 (T8200, Solarbio, Shanghai, China) for 15-30 min and treatment with 0.25% Tween 20 (9005-64-5, Sangon Biotech, Shanghai, China) in DPBS under mineral oil (M8410) for 30 min. The oocytes and embryos were then incubated with 2% BSA (A6003) in DPBS for 1 h at room temperature to block nonspecific binding sites. Immunostaining was performed by incubation with the primary antibody for Nanog (1:2000 dilution; 4893s; Cell Signaling Technology, Boston, MA, USA), H3K4me3 (1:1000 dilution;

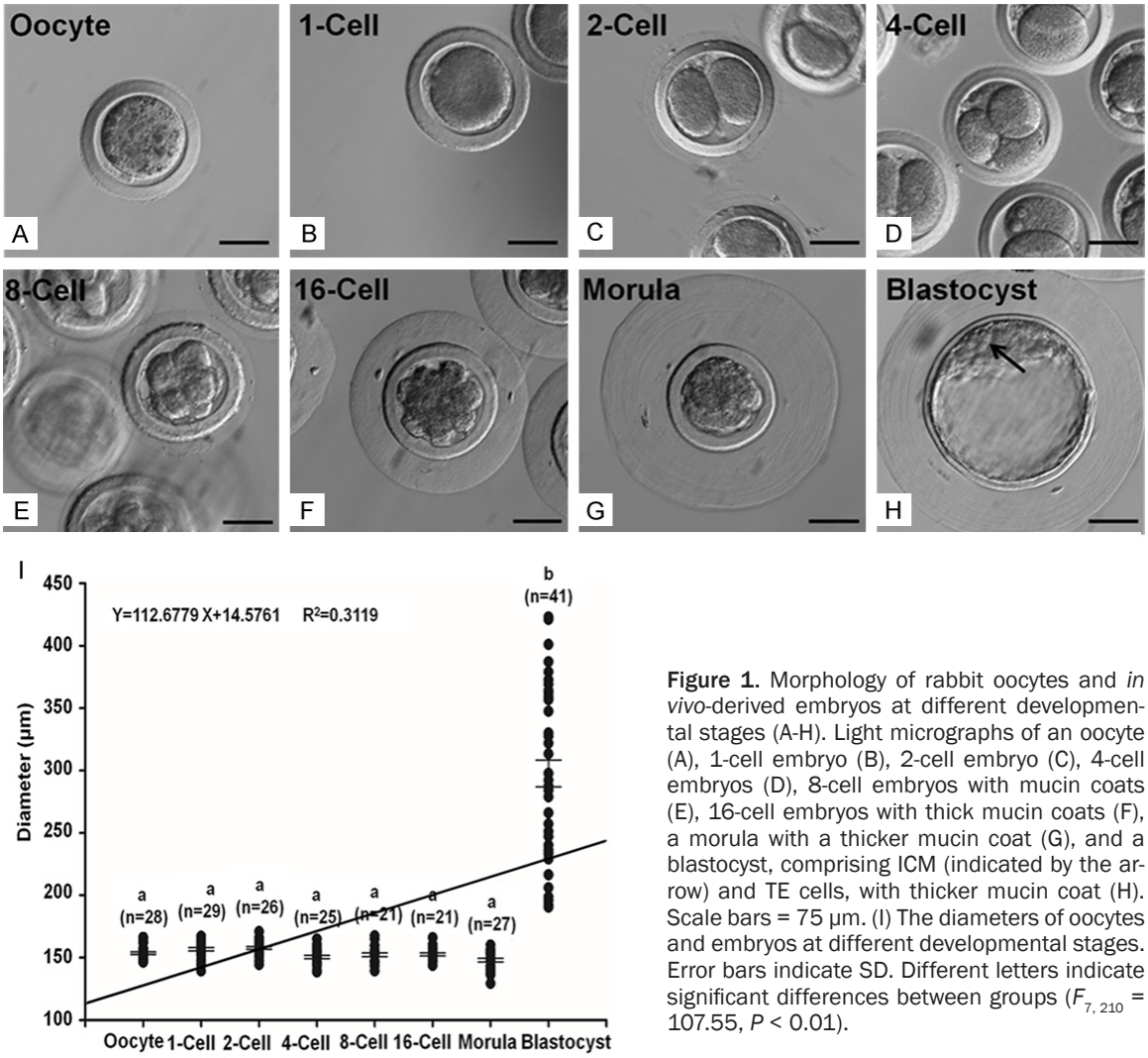

Figure 1. Morphology of rabbit oocytes and *in vivo*-derived embryos at different developmental stages (A-H). Light micrographs of an oocyte (A), 1-cell embryo (B), 2-cell embryo (C), 4-cell embryos (D), 8-cell embryos with mucin coats (E), 16-cell embryos with thick mucin coats (F), a morula with a thicker mucin coat (G), and a blastocyst, comprising ICM (indicated by the arrow) and TE cells, with thicker mucin coat (H). Scale bars = 75 μm. (I) The diameters of oocytes and embryos at different developmental stages. Error bars indicate SD. Different letters indicate significant differences between groups ($F_{7, 210}$ = 107.55, P < 0.01).

ab6000, Abcam Trading (Shanghai) Company Ltd. Pudong, Shanghai, China), or H3K27me3 (1:200 dilution, ab6002, Abcam Trading (Shanghai) Company Ltd. Pudong, Shanghai, China) in DPBS supplemented with 2% FBS overnight at 4°C. The oocytes and embryos were washed in PBST 3 times for 5 min at room temperature and then incubated with secondary antibody Alexa Fluor 488 goat anti-mouse IgG (H+L) (1:200 dilution; Msaf48801, FMS, Nanjing, China) for 2 h at 37°C. Oocytes and embryos were washed in PBST for 30 min at room temperature and then stained with 100 ng/ml DAPI (SN321-1-1, Shengxing Biological, Nanjing, China) for 10 min at room temperature. Finally, oocytes and embryos were mounted on slides with 50% glycerol (G2025) in DPBS. The mounted cells were observed under a fluorescence microscope, and the staining intensity was measured using Image-Pro Insight software (version 8.0; Madia Cybernetics). Nuclear staining of Nanog, H3K4me3, and H3K27me3 was deemed positive for oocytes and embryos that had visible fluorescence in the nuclei/chromosomes. In other words, nuclear fluorescence was assessed as either positive or negative for each oocyte and embryo, some oocytes or embryos with cytoplasm staining were judged as negative if nuclei/chromosomes were not clearly stained.

Statistical analysis

All data were analyzed and processed using Statistica version 6.0 (Tulsa, OK, USA). Kolmogorov-Smimov-test was analyzed with the normality of the data, and Bartlett's test method was used to analyze the homogeneity. The

measurement data were expressed by mean ± standard deviation (SD). Analysis was used to compare with the diameters of embryos at different developmental stages by one-way ANOVA and linear regression analysis. One-way ANOVA was used to assess differences between H3K4me3, H3K27me3, and Nanog expression among embryos at different developmental stages. $P < 0.05$ was considered significant.

Results

The morphology and diameter of in vivo-derived rabbit embryos

The average diameters of oocytes, 1-, 2-, 4-, 8-, and 16-cell embryos, morulae, and blastocysts were measured using Image J software. The diameters of oocytes, 1-cell embryos, and 2-cell embryos were 154±5 μm, 157±7 μm, and 158±6 μm, respectively (**Figure 1A-C**). All embryos beyond the 2-cell stage were covered with a layer of mucin coat. The diameters of the embryos at 4-, 8-, and 16-cell stages were 150±7 μm, 152±7 μm, and 153±5 μm, respectively (**Figure 1D-F**), whereas morulae were 148±8 μm in diameter (**Figure 1G**), and blastocysts were 298±68 μm in diameter (**Figure 1H**). The blastocysts were visibly distinguished as inner cell mass (ICM) and trophoectoderm (TE) cells. There was no significant difference in the diameters of oocytes or embryos through the morulae stage ($P > 0.05$), but the average diameter of blastocysts was significantly larger than those of all embryo stages ($P < 0.01$) (**Figure 1I**). Overall, there was a positive correlation between diameter and embryonic stage ($r = 0.5585$).

Dynamics of the H3K4me3 modification

H3K4me3 localized to the nucleus and was absent from the cytoplasm in 100% of MII oocytes (**Figure 2A**). Similarly, in 1-cell (**Figure 2B**), 2-cell (**Figure 2C**), and 4-cell embryos (**Figure 2D**), H3K4me3 was predominantly located in the nucleus, with only scattered staining observed in the cytoplasm (100% positive) ($P > 0.05$). At the 8-cell stage, a portion of examined embryos were negative for nuclear H3K4me3 staining (**Figure 2F**) while 97.2±2.8% of examined 8-cell embryos were H3K4me3-positive (**Figure 2E**). At16-cell stage, a slightly larger proportion of embryos lacked nuclear H3K4me3 staining (**Figure 2H**), with 94.4±2.9% of embryos staining H3K4me3-positive (**Figure 2G**). Morulae exhibited increased loss of nuclear H3K4me3 (**Figure 2J**), with 86.7±1.4% staining H3K4me3-positive (**Figure 2I**), a frequency significantly lower than that in oocytes and embryos between the 1- and 8-cell stages ($P < 0.05$) (**Figure 2M**). Blastocysts exhibited the highest rate of H3K4me3-negative staining (**Figure 2L**), with an H3K4me3-positive frequency of only 76.2± 4.8% (**Figure 2K**), which was significantly lower than that in oocytes and all other stages of embryos ($P < 0.05$). H3K4me3-positive staining frequency was not significantly different between the 8- and 16-cell stages or between 16-cell and morula stages ($P > 0.05$) (**Figure 2M**).

Dynamics of the H3K27me3 modification

H3K27me3 was not detected in oocytes (**Figure 3A** and **3K**) or embryos of the 1-, 2-, 4-, 8-, or 16-cell stages (**Figure 3B-F**, **3K**). However, 25.9±1.7% of morulae were positive for nuclear H3K27me3 staining (**Figure 3G** and **3K**) while most stained negative (**Figure 3H**). The frequency of H3K27me3-positive staining was further increased in blastocysts to 34.2±3.7% (**Figure 3I** and **3K**), with the remaining blastocysts staining negative (**Figure 3J**). The frequencies of H3K27me3-positive staining in both morulae and blastocysts were significantly higher than those in all earlier stages ($P < 0.05$) (**Figure 3K**). In addition, the H3K27me3-positive frequency in blastocysts was significantly higher than that in morulae ($P < 0.05$) (**Figure 3K**).

Dynamic pattern of Nanog expression

The expression of Nanog was undetectable by immunofluorescence microscopy in oocytes (**Figure 4A**) and in embryos at the 1-cell (**Figure 4B**), 2-cell (**Figure 4C**), 4-cell (**Figure 4D**), 8-cell (**Figure 4E**), and 16-cell stages (**Figure 4F**). However, the proportion of morulae exhibiting Nanog expression was dramatically increased to 24.9±5.6% (**Figure 4G**), with the remaining morulae lacking detectable expression (**Figure 4H**). Blastocysts exhibited the highest frequency of Nanog expression, with 36.5±2.8% staining positive (**Figure 4I**), while the remaining blastocysts stained negative (**Figure 4J**). Nanog

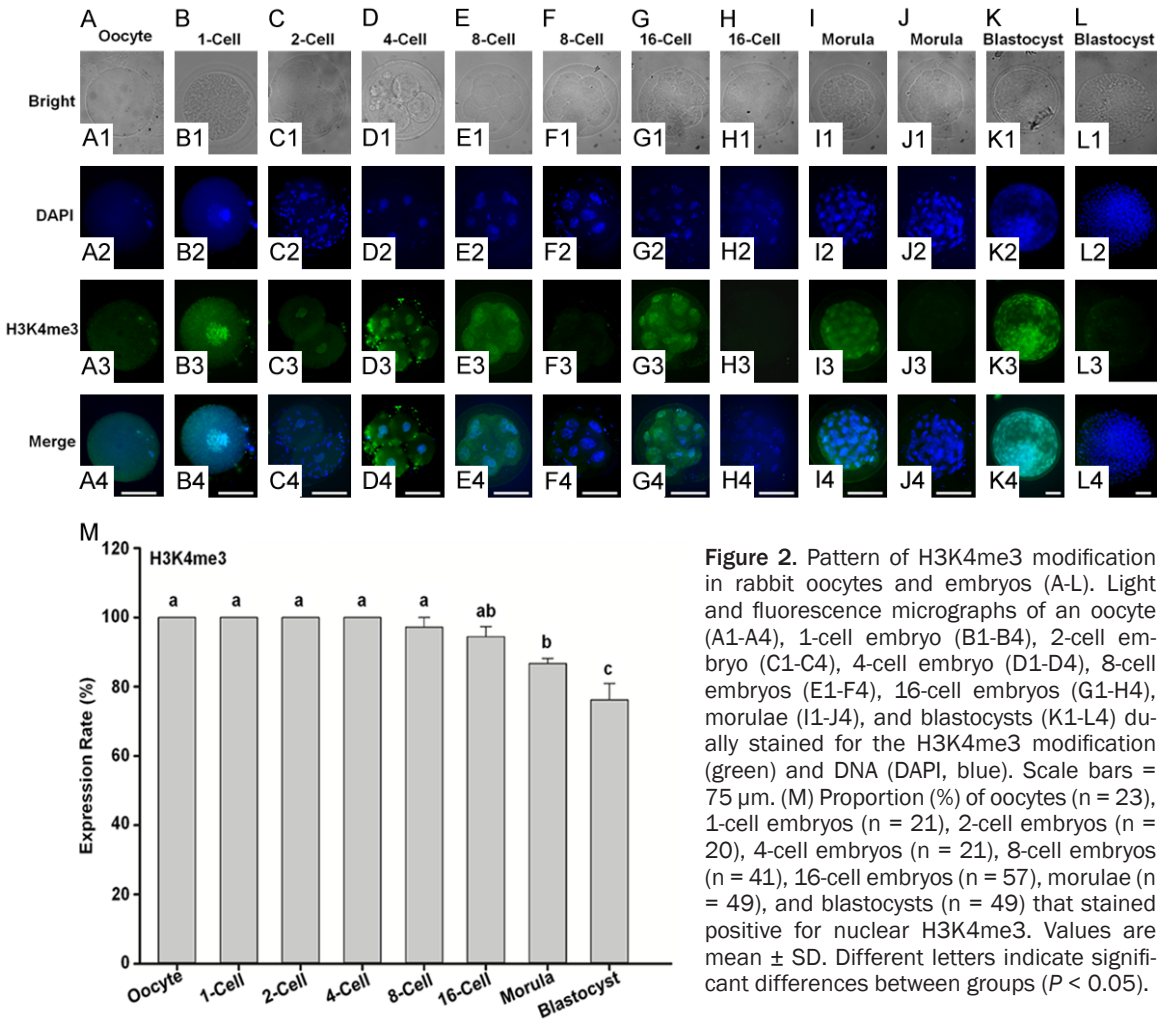

Figure 2. Pattern of H3K4me3 modification in rabbit oocytes and embryos (A-L). Light and fluorescence micrographs of an oocyte (A1-A4), 1-cell embryo (B1-B4), 2-cell embryo (C1-C4), 4-cell embryo (D1-D4), 8-cell embryos (E1-F4), 16-cell embryos (G1-H4), morulae (I1-J4), and blastocysts (K1-L4) dually stained for the H3K4me3 modification (green) and DNA (DAPI, blue). Scale bars = 75 μm. (M) Proportion (%) of oocytes (n = 23), 1-cell embryos (n = 21), 2-cell embryos (n = 20), 4-cell embryos (n = 21), 8-cell embryos (n = 41), 16-cell embryos (n = 57), morulae (n = 49), and blastocysts (n = 49) that stained positive for nuclear H3K4me3. Values are mean ± SD. Different letters indicate significant differences between groups ($P < 0.05$).

was located in both the nucleus and cytoplasm of morulae (**Figure 4G**) and was present throughout the blastocyst, including both the ICM and TE; however, Nanog was primarily located in the ICM of blastocysts, as indicated by the higher staining intensity in the ICM compared to the TE cells (**Figure 4I**). Additionally, although Nanog was present in both the nucleus and cytoplasm of the blastocyst, the nucleus exhibited stronger staining (**Figure 4I**). The frequencies of Nanog expression in morulae and blastocysts were higher than those in all earlier stages, and the Nanog-positive frequency in blastocysts was significantly higher than that in morulae ($P < 0.05$) (**Figure 4K**).

Discussion

Our study has revealed epigenetic modification dynamics of H3K4me3 and H3K27me3 and dynamic expression of a key pluripotent regulatory protein, Nanog, during early development of *in vivo*-derived rabbit embryos. Embryos undergo intense epigenetic reprogramming after fertilization, and the expression of pluripotent regulatory factors regulates the developmental potential and lineage differentiation of embryonic cells [24, 25]. Histone H3 is essential for embryonic development and chromosomal remodeling after fertilization [26, 27]. The modification of several lysine residues in H3 (H3K4, H3K9, H3K27, H3K36) is regulated by histone methyltransferases and demethylases [28, 29] and is necessary for embryo development at various stages, from acquisition of pluripotency by the embryo after fertilization to multi-lineage differentiation after implantation [13, 30]. Among these modifications, H3K4me3 and H3K27me3 are critical for initiating the classical regulatory processes of either activating or

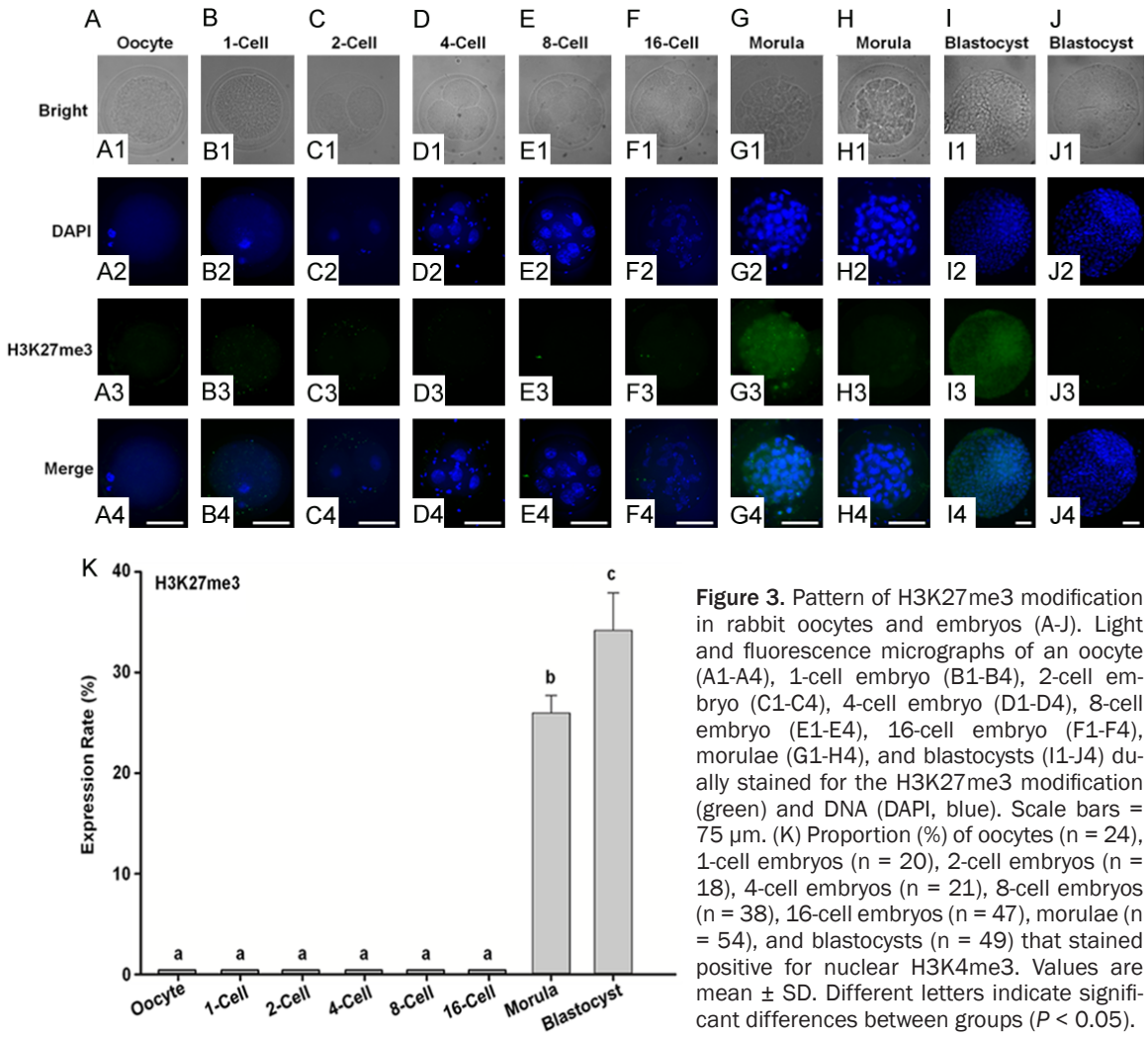

Figure 3. Pattern of H3K27me3 modification in rabbit oocytes and embryos (A-J). Light and fluorescence micrographs of an oocyte (A1-A4), 1-cell embryo (B1-B4), 2-cell embryo (C1-C4), 4-cell embryo (D1-D4), 8-cell embryo (E1-E4), 16-cell embryo (F1-F4), morulae (G1-H4), and blastocysts (I1-J4) dually stained for the H3K27me3 modification (green) and DNA (DAPI, blue). Scale bars = 75 μm. (K) Proportion (%) of oocytes (n = 24), 1-cell embryos (n = 20), 2-cell embryos (n = 18), 4-cell embryos (n = 21), 8-cell embryos (n = 38), 16-cell embryos (n = 47), morulae (n = 54), and blastocysts (n = 49) that stained positive for nuclear H3K4me3. Values are mean ± SD. Different letters indicate significant differences between groups ($P < 0.05$).

suppressing gene expression [4, 5]. We found that H3K4me3 decreased overall during preimplantation embryo development. All examined oocytes and 1-, 2-, and 4-cell embryos were positive for nuclear H3K4me3, but its occurrence decreased slightly among 8-cell embryos and decreased significantly in morulae (86.7%) and blastocysts (76.2%). A recent model proposes that H3K4me3 is located as a broad peak at promoter regions and at various distal sites, whereas the classical model postulates that H3K4me3 is located only in the CpG-rich regions of promoters [4]. This new model indicates a more important role for H3K4me3 in embryo development and differentiation. In mice, H3K4me3 is highly elevated in oocytes, following the erasure of a non-canonical form of H3K4me3 on the maternal genome of mature oocytes and rapid replacement with the H3K4me3 modification in late 2-cell embryos, in accordance with the timing of zygotic genome activation (ZGA) [4, 5, 26]. The erasure of non-canonical H3K4me3 is necessary to direct the process of ZGA, while replacement with typical H3K4me3 activates the expression of several development-related genes [5, 26]. Our results indicated that rabbit oocytes and embryos prior to the 4-cell stage possess a high nuclear abundance of H3K4me3, with levels declining from the 8-cell stage onward. This trend differs slightly from that reported in 2-cell mouse embryos, but the observed reduction beginning at the 8-cell stage is in accordance with rabbit embryonic ZGA [5, 26].

In contrast to H3K4me3, H3K27me3 was not observed in oocytes or any embryos between the 1- and 16-cell stages, but H3K27me3 occurrence dramatically increased in morulae and reached the highest level in blastocysts

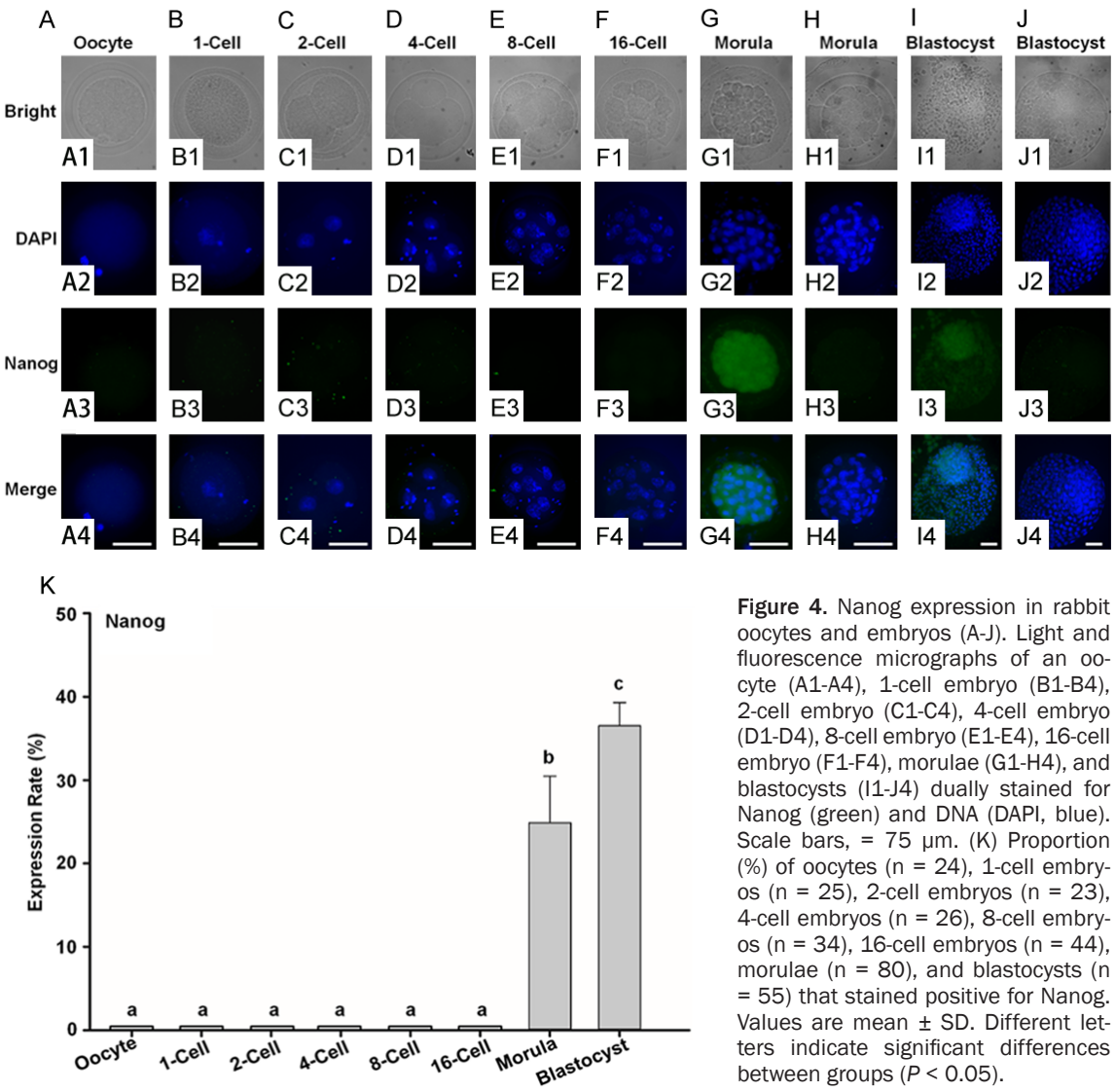

Figure 4. Nanog expression in rabbit oocytes and embryos (A-J). Light and fluorescence micrographs of an oocyte (A1-A4), 1-cell embryo (B1-B4), 2-cell embryo (C1-C4), 4-cell embryo (D1-D4), 8-cell embryo (E1-E4), 16-cell embryo (F1-F4), morulae (G1-H4), and blastocysts (I1-J4) dually stained for Nanog (green) and DNA (DAPI, blue). Scale bars, = 75 μm. (K) Proportion (%) of oocytes (n = 24), 1-cell embryos (n = 25), 2-cell embryos (n = 23), 4-cell embryos (n = 26), 8-cell embryos (n = 34), 16-cell embryos (n = 44), morulae (n = 80), and blastocysts (n = 55) that stained positive for Nanog. Values are mean ± SD. Different letters indicate significant differences between groups ($P < 0.05$).

(34.2%). The localization of H3K27me3 and DNA methylation is highly related to transcriptional silencing [4]. H3K27me3 is widely distributed in a non-canonical pattern among intergenic spacers and gene deserts [5]. After fertilization, H3K27me3 is largely removed from the promoter regions of development-related genes. As recently reported, paternal (i.e., sperm) H3K27me3 is erased but the H3K27me3 in distal regions of maternal (i.e., oocyte) promoters is retained [5, 26]. This allele-specific pattern of differential H3K27me3 modification persists from the fertilized egg until the blastocyst stage [4, 5, 26]. It has been reported that the Polycomb complex is responsible for catalyzing the formation of H3K27me3, and H3K27me3 deposition represses the expression of numerous development-related genes [31, 32]. However, there is evidence that the promoter regions of such development-related genes and specific chromatin states can be bivalently modified with both H3K4me3 and H3K27me3 in early embryos [33]. Bivalent H3K27me3 and H3K4me3 methylation also occurs in the promoters of mesendoderm-specific genes [33]. The genes with bivalent modification are usually responsible for embryo development and differentiation [33], and expression of these genes is low in undifferentiated ESC but rapidly induced in embryonic cells in response to differentiation signals [33]. In addition, bivalent H3K4me3 and H3K27me3 modification occurs in the promoter regions of post-implantation-related genes during ICM-specific

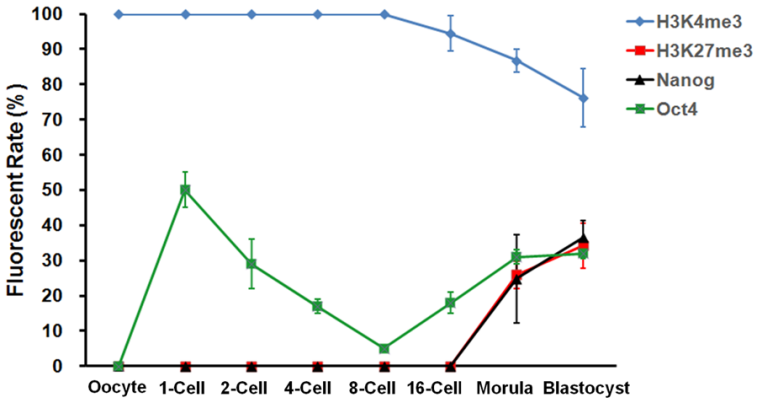

Figure 5. Expression patterns of H3K4me3 and H3K27me3 modifications and Oct4 and Nanog proteins in early rabbit oocytes and embryos. The proportion (%) of oocytes, 1-cell embryos, 2-cell embryos, 4-cell embryos, 8-cell embryos, 16-cell embryos, morulae, and blastocysts staining positive for H3K4me3, H3K27me3, Oct4, or Nanog. Oct4 nuclear expression data was derived from our previously published studies [18].

lineage differentiation, indicating that this bivalent modification is closely related to post-implantation development.

In this study, the H3K27me3 modification was not detected prior to the 16-cell stage but increased in abundance in morulae and reached the highest levels in blastocysts; in contrast, H3K4me3 began to decline in 8-cell embryos. These results indicated that the morulae and blastocysts carried both H3K4me3 and H3K27me3 modifications. We noticed, however, that the decline of H3K4me3 (8-cell stage) preceded the increase of H3K27me3 (morulae stage) in rabbit embryos [4]. In mice, H3K27me3 begins to rise after the blastocyst stage, and the conversion from non-canonical to typical H3K27me3 modification indicates that lineage differentiation occurs in blastocysts [5, 26]. The increase of H3K27me3 in rabbit morulae suggest that the embryonic cells in morulae have undergone lineage differentiation. We believe that an equilibrium of H3K4me3 and H3K27me3 modifications in rabbit blastocysts may be functionally similar to bivalent modification in mouse blastocysts [4, 5, 26]. This equilibrium may enable embryos to precisely control expression of differentiation-related genes, subsequently allowing the determination of lineage fate in response to time-dependent developmental events [4, 5, 26]. Although rabbit embryos showed different histone H3 reprogramming patterns than mouse embryos, the detailed patterns of H3K4me3 and H3K27me3 modification and transition between non-canonical and typical modifications in rabbit embryos remain unclear. Future work, perhaps using high-resolution histone-modification specific ChIP-Seq will be important to gain a more comprehensive understanding of H3K4me3, H3K27me3, and other epigenetic information in developmental genes and specific chromatin states during rabbit embryo development. Such information will be invaluable for understanding the differences and similarities in embryo development among different species, including reprogramming events in human embryos.

In this study, Nanog expression followed a pattern similar to that of H3K27me3, wherein it was not expressed in oocytes or embryos between the 1- and 16-cell stage, but its occurrence increased in morulae (24.9% positive) and reached the highest level in blastocysts (36.5% positive). To the best of our knowledge, there is no prior report describing Nanog expression in *in vivo*-derived rabbit embryos. Our previous study revealed that the expression of *Oct4*, another pluripotency gene, gradually increased following the 8-cell stage (**Figure 5**), although the maternal Oct4 signal in the nuclei of embryos initially decreased prior to the 8-cell stage [18]. In oocytes, Oct4 was not detected in the nuclei of MII oocytes but rather was distributed in the cytoplasm [18]. However, the expression of Oct4 is complex, and although Oct4 was expressed throughout the early blastocysts, its expression was higher in the ICM than in TE cells [18]. Furthermore, in the expanded blastocyst, Oct4 expression in the ICM and TE are simultaneously downregulated, and although expression rapidly resumes in the ICM of hatching blastocysts, its expression in TE cells remains off or occurs at very low levels. In this study, we found that Nanog was expressed throughout the rabbit embryo, similar to Oct4, with higher expression in the ICM than in TE cells in Day 4 blastocysts. It remains to be determined if late stage (Day 5) rabbit blastocysts exhibit the same pattern. It is evident from these results that Nanog gene expression, which initiates at the morula stage,

follows the onset of Oct4 expression and rabbit ZGA at the 8-cell stage [18]. Oct4, as a transcription factor, can bind to the promotor region of the *Nanog* gene and, in turn, activate *Nanog* transcription [34-36]. It is reported that Nanog expression occurs primarily in early embryos, ESC, and embryonic tumor cells [21, 37] but not in more differentiated cells, such as hematopoietic stem cells, luminal endoderm, and differentiated ESC [38]. The removal of *Nanog* results in the differentiation of ESC into primitive endoderm-like cells but does not affect the differentiation of early embryonic trophoblasts [39]. It is believed that when both pluripotency genes, *Oct4* and *Nanog*, are expressed, they can, in turn, activate other corresponding developmental genes to enable cell repro gramming [40, 41]. Our results in Nanog expression are in support of those previously published results. In addition, we observed similar pattern between Nanog and H3K27me3. It will be interesting to test whether they appeared in the same embryos and what is the mechanism governing this association.

The dynamic expression patterns of Oct4, Nanog, and the H3K4me3 and H3K27me3 modifications in rabbit embryos (**Figure 5**) provide important information for the derivation of naïve rabbit ESC [18]. Pluripotent rabbit ESC were first derived many years ago, but, to date, no rabbit ESC line has been proven capable of germ-line transmission [16, 42-44]. In ESC, the methylation of H3K4 and H3K27 regulates transcription and determines ESC fate [32, 33, 45-49], and epigenetic factors can regulate mouse ESC self-renewal [50]. Histone modification studies have shown that bivalent H3K4me3 and H3K27me3 modification in ICM resembles that of ESC [4]. Nanog, together with other factors, such as Oct4, Klf4, and Sox2, plays an important role in maintaining ESC self-renewal, proliferation, and naïve pluripotency. Co-expression of Nanog and Oct4 is beneficial to derive and maintain ESC [34, 45], and we predict that rabbit ESC can be derived from embryos expressing higher levels of Nanog and Oct4.

Cloned embryos derived by somatic cell nuclear transfer (NT) possess much lower rate of developmental success [51], and the patterns of histone modification are highly disruptive [52, 53], with epigenetic abnormalities such as DNA methylation [52, 53]. and abnormal patterns of H3K9me3 posing major barriers for successful cloning [52, 53]. Specifically, gene activation in NT embryos is hindered due to incomplete erasure of H3K9me3 in donor nuclei, resulting in an arrested development of NT embryos. Overexpression of the H3K9me3-specific demethylase, Kdm4d, in early NT embryos can greatly increase the rates of NT blastocyst production (> 90%) and birth of cloned mice [52, 53]. It is reported that loss of H3K27me3 imprinting in cloned embryos will disrupt post-implantation development, which is another barrier for embryo development to terms [54]. Our study in normal rabbit embryo can provide a good reference for studying the development of rabbit cloned embryos. It will be interesting to see the dynamics of histone modification and pluripotent factors in rabbit NT embryos.

In summary, we used immunofluorescence staining to reveal the dynamic expression profiles of H3K4me3, H3K27me3, and Nanog during development of *in vivo*-derived rabbit embryos. H3K4me3 abundance declined at the 8-cell stage whereas H3K27me3 increased after the 16-cell stage. Nanog expression also increased specifically after the 16-cell stage. At the blastocyst stage, H3K4me3, H3K27me3, and Nanog expression rates reached 76.2%, 34.2%, and 36.5%, respectively. This equilibrium pattern in *in vivo*-derived rabbit embryos provides an important molecular and epigenetic profile for rabbit pre-implantation embryos, which will be using for deriving authentic rabbit ESC and improving the efficiency of rabbit somatic cell NT.

Acknowledgements

The authors greatly appreciated Dr. Falong Lu at Institute of Genetics and Developmental Biology, Chinese Academy of Sciences for critical reading and comments. This study was supported in part by grants from the National Natural Science Foundation of China (31471388 and 31701285), China Postdoctoral Science Foundation (2018M632330), and Priority Academic Program Development of Jiangsu Higher Education Institutions to FD.

Disclosure of conflict of interest

None.

Address correspondence to: Dr. Fuliang Du, Jiangsu Key Laboratory for Molecular and Medical Biotechnology, College of Life Sciences, Nanjing Normal University, #1 Wenyuan Rd, Nanjing 210046, PR China. Tel: +86-25-85898011; E-mail: fuliangd@njnu.edu.cn

References

[1] Gu TP, Guo F, Yang H, Wu HP, Xu GF, Liu W, Xie ZG, Shi L, He X and Jin SG. The role of Tet3 DNA dioxygenase in epigenetic reprogramming by oocytes. Nature 2011; 477: 606-610.

[2] Guo F, Li X, Liang D, Li T, Zhu P, Guo H, Wu X, Wen L, Gu TP, Hu B, Walsh CP, Li J, Tang F, Xu GL. Active and passive demethylation of male and female pronuclear DNA in the mammalian zygote. Cell Stem Cell 2014; 15: 447-458.

[3] Wu J, Huang B, Chen H, Yin Q, Liu Y, Xiang Y, Zhang B, Liu B, Wang Q and Xia W. The landscape of accessible chromatin in mammalian preimplantation embryos. Nature 2016; 534: 652.

[4] Liu X, Wang C, Liu W, Li J, Li C, Kou X, Chen J, Zhao Y, Gao H and Wang H. Distinct features of H3K4me3 and H3K27me3 chromatin domains in pre-implantation embryos. Nature 2016; 537: 558-562.

[5] Zheng H, Huang B, Zhang B, Xiang Y, Du Z, Xu Q, Li Y, Wang Q, Ma J and Peng X. Resetting epigenetic memory by reprogramming of histone modifications in mammals. Mol Cell 2016; 63: 1066-1079.

[6] Wang C, Liu X, Gao Y, Yang L, Li C, Liu W, Chen C, Kou X, Zhao Y and Chen J. Reprogramming of H3K9me3-dependent heterochromatin during mammalian embryo development. Nat Cell Biol 2018; 20: 620-631.

[7] Smith ZD, Chan MM, Humm KC, Karnik R, Mekhoubad S, Regev A, Eggan K and Meissner A. DNA methylation dynamics of the human preimplantation embryo. Nature 2014; 511: 611.

[8] Zhu P, Guo H, Ren Y, Hou Y, Dong J, Li R, Lian Y, Fan X, Hu B and Gao Y. Single-cell DNA methylome sequencing of human preimplantation embryos. Nat Genet 2017; 50: 12.

[9] Wu J, Xu J, Liu B, Yao G, Wang P, Lin Z, Huang B, Wang X, Li T and Shi S. Chromatin analysis in human early development reveals epigenetic transition during ZGA. Nature 2018; 557: 256-260.

[10] Lachner M, O'Carroll D, Rea S, Mechtler K and Jenuwein T. Methylation of histone H3 lysine 9 creates a binding site for HP1 proteins. Nature 2001; 410: 116-120.

[11] Wang J, Hevi S, Kurash JK, Lei H, Gay F, Bajko J, Su H, Sun W, Chang H and Xu G. The lysine demethylase LSD1 (KDM1) is required for maintenance of global DNA methylation. Nat Genet 2009; 41: 125-129.

[12] Xie R, Everett LJ, Lim HW, Patel NA, Schug J, Kroon E, Kelly OG, Wang A, D'Amour KA and Robins AJ. Dynamic chromatin remodeling mediated by Polycomb proteins orchestrates pancreatic differentiation of human embryonic stem cells. Cell Stem Cell 2013; 12: 224.

[13] Xie W, Schultz M, Lister R, Hou Z, Rajagopal N, Ray P, Whitaker J, Tian S, Hawkins RD and Leung D. Epigenomic analysis of multilineage differentiation of human embryonic stem cells. Cell 2013; 153: 1134.

[14] Fan J and Watanabe T. Transgenic rabbits as therapeutic protein bioreactors and human disease models. Pharmacol Ther 2003; 99: 261.

[15] Fan J, Kitajima S, Watanabe T, Xu J, Zhang J, Liu E and Chen YE. Rabbit models for the study of human atherosclerosis: from pathophysiological mechanisms to translational medicine. Pharmacol Ther 2015; 146: 104-119.

[16] Intawicha P, Ou YW, Lo NW, Zhang SC, Chen YZ, Lin TA, Su HL, Guu HF, Chen MJ, Lee KH, Chiu YT, Ju JC. Characterization of embryonic stem cell lines derived from New Zealand white rabbit embryos. Cloning Stem Cells 2009; 11: 27-38.

[17] Lin TA, Chen CH, Sung LY, Carter MG, Chen YE, Du F, Ju JC and Xu J. Open-pulled straw vitrification differentiates cryotolerance of in vitro cultured rabbit embryos at the eight-cell stage. Theriogenology 2011; 75: 760-768.

[18] Chen CH, Chang WF, Liu CC, Su HY, Shyue SK, Cheng WT, Chen YE, Wu SC, Du F and Sung LY. Spatial and temporal distribution of Oct-4 and acetylated H4K5 in rabbit embryos. Reprod Biomed Online 2012; 24: 433-442.

[19] Lepikhov K, Zakhartchenko V, Ru H, Yang F, Wrenzycki C, Niemann H, Wolf E and Walter J. Evidence for conserved DNA and histone H3 methylation reprogramming in mouse, bovine and rabbit zygotes. Epigenetics Chromatin 2008; 1: 8.

[20] Chen CH, Xu J, Chang WF, Liu CC, Su HY, Chen YE, Du F and Sung LY. Dynamic profiles of Oct-4, Cdx-2 and acetylated H4K5 in in-vivo-derived rabbit embryos. Reprod Biomed Online 2012; 25: 358-370.

[21] Ezeh UI, Turek PJ, Reijo RA and Clark AT. Human embryonic stem cell genes OCT4, NANOG, STELLAR, and GDF3 are expressed in both seminoma and breast carcinoma. Cancer 2010; 104: 2255-2265.

[22] Pashaiasl M, Khodadadi K, Kayvanjoo AH, Pashaei-Asl R, Ebrahimie E and Ebrahimi M. Unravelling evolution of Nanog, the key transcription factor involved in self-renewal of undifferentiated embryonic stem cells, by pattern

recognition in nucleotide and tandem repeats characteristics. Gene 2016; 578: 194-204.
[23] Du F, Xu J, Zhang J, Gao S, Carter MG, He C, Sung LY, Chaubal S, Fissore RA and Tian XC. Beneficial effect of young oocytes for rabbit somatic cell nuclear transfer. Cloning Stem Cells 2009; 11: 131-140.
[24] Rivera RM and Ross JW. Epigenetics in fertilization and preimplantation embryo development. Prog Biophys Mol Biol 2013; 113: 423-432.
[25] Inoue A, Jiang L, Lu F, Suzuki T and Zhang Y. Maternal H3K27me3 controls DNA methylation-independent imprinting. Nature 2017; 547: 419-424.
[26] Zhang B, Zheng H, Huang B, Li W, Xiang Y, Xu P, Jia M, Wu X, Zhang Y and Xu Q. Allelic reprogramming of the histone modification H3K4me3 in early mammalian development. Nature 2016; 537: 553-557.
[27] Kong Q, Banaszynski LA, Geng F, Zhang X, Zhang J, Zhang H, O'Neill CL, Yan P, Liu Z and Shido K. Histone variant H3.3-mediated chromatin remodeling is essential for paternal genome activation in mouse preimplantation embryos. J Biol Chem 2018; 293: 3829-3838.
[28] Cyrus M and Yi Z. The diverse functions of histone lysine methylation. Nat Rev Mol Cell Biol 2005; 6: 838.
[29] Klose RJ, Kallin EM and Yi Z. JmjC-domain-containing proteins and histone demethylation. Nat Rev Genet 2006; 7: 715-727.
[30] Nakanishi MO, Hayakawa K, Nakabayashi K, Hata K, Shiota K and Tanaka S. Trophoblast-specific DNA methylation occurs after the segregation of the trophectoderm and inner cell mass in the mouse periimplantation embryo. Epigenetics 2012; 7: 173-182.
[31] Boyer LA, Plath K, Zeitlinger J, Brambrink T, Medeiros LA, Lee TI, Levine SS, Wernig M, Tajonar A and Ray MK. Polycomb complexes repress developmental regulators in murine embryonic stem cells. Nature 2006; 441: 349-353.
[32] Lee TI, Jenner RG, Boyer LA, Guenther MG, Levine SS, Kumar RM, Chevalier B, Johnstone SE, Cole MF and Isono K. Control of developmental regulators by polycomb in human embryonic stem cells. Cell 2006; 125: 301.
[33] Bernstein BE, Mikkelsen TS, Xie X, Kamal M, Huebert DJ, Cuff J, Fry B, Meissner A, Wernig M and Plath K. A bivalent chromatin structure marks key developmental genes in embryonic stem cells. Cell 2006; 125: 315-326.
[34] Loh YH, Wu Q, Chew JL, Vega VB, Zhang W, Chen X, Bourque G, George J, Leong B and Liu J. The Oct4 and Nanog transcription network regulates pluripotency in mouse embryonic stem cells. Nat Genet 2006; 38: 431-440.
[35] Wolf XA, Serup P and Hyttel P. Three-dimensional localisation of NANOG, OCT4, and E-cadherin in porcine pre- and peri-implantation embryos. Dev Dyn 2011; 240: 204-210.
[36] Cai SZ, Fang-Fei LI and Wang YP. Transcription factors Oct4 and Nanog and related regulatory network maintain the characteristics of pluripotent stem cells. Progress of Anatomical Sciences 2011.
[37] van den Berg DL, Zhang W, Yates A, Engelen E, Takacs K, Bezstarosti K, Demmers J, Chambers I, Poot RA. Estrogen-related receptor beta interacts with Oct4 to positively regulate nanog gene expression. Mol Cell Biol 2008; 28: 5986-95.
[38] Hyslop L, Stojkovic M, Armstrong L, Walter T, Stojkovic P, Przyborski S, Herbert M, Murdoch A, Strachan T and Lako M. Downregulation of NANOG induces differentiation of human embryonic stem cells to extraembryonic lineages. Stem Cells 2005; 23: 1035-1043.
[39] Hart AH, Hartley L, Ibrahim M and Robb L. Identification, cloning and expression analysis of the pluripotency promoting Nanog genes in mouse and human. Dev Dyn 2004; 230: 187.
[40] Miyamoto T, Furusawa C and Kaneko K. Pluripotency, differentiation, and reprogramming: a gene expression dynamics model with epigenetic feedback regulation. PLoS Comput Biol 2015; 11: e1004476.
[41] Medvedev SP, Shevchenko AI, Mazurok NA and Zakiian SM. [OCT4 and NANOG are the key genes in the system of pluripotency maintenance in mammalian cells]. Genetika 2008; 44: 1589.
[42] Graves KH and Moreadith RW. Derivation and characterization of putative pluripotential embryonic stem cells from preimplantation rabbit embryos. Mol Reprod Dev 2010; 36: 424-433.
[43] Schoonjans L, Albright GM, Li JL, Collen D and Moreadith RW. Pluripotential rabbit embryonic stem (ES) cells are capable of forming overt coat color chimeras following injection into blastocysts. Mol Reprod Dev 2015; 45: 439-443.
[44] Du F, Chen CH, Li Y, Hu Y, An LY, Yang L, Zhang J, Chen YE and Xu J. Derivation of rabbit embryonic stem cells from vitrified-thawed embryos. Cell Reprogram 2015; 17: 453.
[45] Boyer LA, Tong IL, Cole MF, Johnstone SE, Levine SS, Zucker JP, Guenther MG, Kumar RM, Murray HL and Jenner RG. Core transcriptional regulatory circuitry in human embryonic stem cells. Cell 2005; 122: 947.
[46] Guenther MG, Levine SS, Boyer LA, Jaenisch R and Young RA. A chromatin landmark and transcription initiation at most promoters in human cells. Cell 2007; 130: 77-88.

[47] Guenther MG, Frampton GM, Soldner F, Hockemeyer D, Mitalipova M, Jaenisch R and Young RA. Chromatin structure and gene expression programs of human embryonic and induced pluripotent stem cells. Cell Stem Cell 2010; 7: 249-257.

[48] Azuara V, Perry P, Sauer S, Spivakov M, Jørgensen HF, John RM, Gouti M, Casanova M, Warnes G and Merkenschlager M. Chromatin signatures of pluripotent cell lines. Nat Cell Biol 2006; 8: 532-538.

[49] Mikkelsen TS, Ku M, Jaffe DB, Issac B, Lieberman E, Giannoukos G, Alvarez P, Brockman W, Kim TK and Koche RP. Genome-wide maps of chromatin state in pluripotent and lineage-committed cells. Nature 2007; 448: 553.

[50] He J, Shen L, Wan M, Taranova O, Wu H and Zhang Y. Kdm2b maintains murine embryonic stem cell status by recruiting PRC1 complex to CpG islands of developmental genes. Nat Cell Biol 2013; 15: 373-384.

[51] Jullien J, Pasque V, Halleystott RP, Miyamoto K and Gurdon JB. Mechanisms of nuclear reprogramming by eggs and oocytes: a deterministic process? Nat Rev Mol Cell Biol 2011; 12: 453-459.

[52] Matoba S, Liu Y, Lu F, Iwabuchi KA, Shen L, Inoue A, Zhang Y. Embryonic development following somatic cell nuclear transfer impeded by persisting histone methylation. Cell 2014; 159: 884-895.

[53] Liu W, Liu X, Wang C, Gao Y, Rui G, Kou X, Zhao Y, Li J, You W and Xiu W. Identification of key factors conquering developmental arrest of somatic cell cloned embryos by combining embryo biopsy and single-cell sequencing. Cell Discov 2016; 2: 16010.

[54] Matoba S, Wang H, Lan J, Lu F, Iwabuchi KA, Wu X, Inoue K, Lin Y, Press W and Lee JT. Loss of H3K27me3 imprinting in somatic cell nuclear transfer embryos disrupts post-implantation development. Cell Stem Cell 2018; 23: 343.